Conductivity peak, relaxation dynamics, and superconducting gap of $YBa_2Cu_3O_7$ studied by terahertz and femtosecond optical spectroscopies

A. Frenkel,* F. Gao,† Y. Liu, J. F. Whitaker, and C. Uher
Center for Ultrafast Optical Science, University of Michigan, Ann Arbor, Michigan 48109

S. Y. Hou and J. M. Phillips‡
AT&T Bell Laboratory, Murray Hill, New Jersey 07974
(Received 11 September 1995)

Recent measurements at microwave, terahertz (THz), and infrared frequencies have revealed a peak in σ_1 below T_c. Based on our THz measurements, which were performed on high quality, single crystal films of YBCO (900 and 500 Å), we have found that σ_1 features a peak which increases in amplitude and shifts to lower temperatures as frequency changes from 1.2 to 0.4 THz. Although the quasiparticle relaxation time extracted from these results using the two-fluid Drude model exhibits an enhancement below T_c, the analysis may not be adequate to account for the strong frequency dependence of the conductivity peak by the competition between the drop in scattering rate and the decreasing normal fluid density with temperature. On the contrary, we were able to account for the frequency dependent σ_1 by fitting with Mattis-Bardeen theory (modified to include scattering) using a slower average rate of increase of the anisotropic gap than for the BCS case as temperature decreases below T_c. This is consistent with the higher normal fluid density (higher than Gorter-Casimir values) from the two-fluid model interpretation of our THz results. Thus, we have found evidence of BCS coherence factors in a high-T_c superconductor with a slower than BCS gap increase below T_c. We have discussed the role of coherence factors to account for the presence of the conductivity peak and the absence of the peak in NMR relaxation rate. Furthermore, we have presented a model for the quasiparticle relaxation time measured by the femtosecond pump-probe spectroscopy. This model allowed us to find a fit to the temperature-dependent energy gap function which is also consistent with the slower gap increase below T_c. In addition, recent theoretical developments based on an anisotropic *s*-wave gap [A. Sudbø *et al.*, Phys. Rev. B **49**, 12 245 (1994)] coincide with our conclusion about the slower gap change below T_c. [S0163-1829(96)06225-X]

I. INTRODUCTION

Measurements of the temperature- and frequency-dependent conductivity (σ_1) in superconductors have played a major role in understanding and establishing the mechanism of conventional BCS superconductivity.[1] The real part of conductivity, σ_1, is a measure of excitation of quasiparticles caused by the absorption of photons of energy $\hbar\omega$. For temperatures close to zero, conventional low-temperature superconductors (LTS's) have shown a vanishing real conductivity up to a threshold frequency $\hbar\omega=2\Delta$, where 2Δ is the BCS energy gap on the order of terahertz (THz) frequencies.[2] As temperature is increased, the σ_1 at $\hbar\omega<2\Delta$ is no longer zero due to the presence of thermally excited quasiparticles. Moreover, due to the correlation between scattering of quasiparticles involving spin-independent constructive interaction associated with paired wave functions, BCS theory predicts that the temperature-dependent conductivity at $\hbar\omega\ll 2\Delta$ exhibits a coherence peak typically at the temperature $T=(0.8-0.9)T_c$.[3] It also predicts similar coherent effects in the nuclear relaxation $1/T_1$ (Hebel-Slichter peak) observed in LTS.[4,5] Here, coherent factors are due to the correlation between scattering events of quasiparticles of opposite momentum and spin (involving hyperfine coupling of quasiparticle relaxation to nuclear spin relaxation).

Since the discovery of high-temperature superconductors (HTS's) researchers have looked for evidence of coherence peaks to identify BCS-like behavior. A ''coherencelike'' peak in σ_1 has been observed using microwave,[6,7] terahertz,[8] and infrared[9,10] techniques in HTS. On the other hand, the Hebel-Slichter peak in the nuclear relaxation rate has been consistently absent in NMR experiments with HTS.[11–14] Different explanations have been proposed to account for this controversy. We name just a few of them. For example, Marsiglio,[15] by ruling out the clean limit as well as strong coupling, has been unable to produce a coherence peak in σ_1 while producing none in $1/T_1$, thus suggesting that some other effects (nonintrinsic to superconductivity) are responsible for the observed lack of a peak in $1/T_1$. Atkins and Carbotte[16] have shown that the coherence peak in $1/T_1$ is reduced substantially with increasing coupling through the quasiparticle damping effects. Other investigators have suggested that the conductivity peak could be a result of the competition between a rapidly growing lifetime and a decreasing number of quasiparticles as the temperature is lowered below T_c.[6,8,10] Indeed, femtosecond optical spectroscopy measurements using pump-probe techniques showed an increase in the relaxation time below T_c for HTS.[17–21] Other opinions have also been reported. Holczer *et al.*[9] attributed the peak to the consequence of ordinary case-II BCS coherence factors and concluded that the pairing was dominantly *s* wave. Mandrus *et al.*[22] applied the two-fluid model (which does not take into consideration BCS coherence factors) and obtained a continuous *T*-linear drop in quasiparticle scattering rate which did not explain the shift of the conductivity peak below T_c. They concluded that BCS coherent factors

should play a role. Finally, a number of authors attributed suppression of the NMR coherence peak to the anisotropic properties of HTS.[11,23–26]

In this paper we clarify the origin of the peak in σ_1 in relationship to the BCS coherence factors, to the temperature dependence of the energy gap, and to the quasiparticle relaxation rate. We show that σ_1 obtained from our terahertz measurements performed on high-quality single-crystal YBCO thin films (900 and 500 Å) has the peak which increases in amplitude and shifts to lower temperatures as frequency is decreased from 1.2 to 0.4 THz. Although the quasiparticle relaxation time reduced from these results using the two-fluid Drude model shows an enhancement below T_c, it is not enough to explain a strong frequency dependence of the conductivity peak by the competition between the drop in scattering rate and the decreasing normal fluid density with temperature. On the contrary, we have been able to model σ_1 by the Mattis-Bardeen theory using a BCS zero-temperature gap, but with a slower than BCS gap increase when the temperature decreased below T_c. This is consistent with the higher normal fluid density (higher than Gorter-Casimir values) which followed from the two-fluid Drude model interpretation of our THz data. Thus, our results suggest that an anisotropic energy gap with a more slowly increasing gap below T_c is responsible for the ''modification'' (shifting to lower temperatures) of the BCS-like coherence peak in σ_1. We will also discuss the role of coherence factors and anisotropic energy gap to account for the presence of the conductivity peak and the absence of the peak in NMR relaxation rate. Furthermore, we will present a model for the quasiparticle relaxation time measured by the femtosecond pump-probe spectroscopy, where this relaxation time is proportional to the change in the energy gap imposed by the femtosecond pulse. This model has allowed us to find a fit to the temperature-dependent energy gap function which is also consistent with the slower gap increase below T_c.

II. EXPERIMENT

A. Thin-film samples

The YBCO films have been grown epitaxially on 10 mm×10 mm×0.5 mm $LaAlO_3$ (100) wafers using the BaF_2 process.[27] Y, Cu, and BaF_2 are co-evaporated to a substrate with the Y:Ba:Cu stoichiometry controlled to within 1% of 1:2:3, as determined by Rutherford backscattering spectrometry.[28,29] The substrate is not intentionally heated during growth and the films are made superconducting by the use of a two-stage anneal. The resulting films have excellent crystallinity (back-scattered minimum yield of 2% by ion channeling), high critical temperature ($T_c \geqslant 90$ K), and high critical current density ($J_c > 10^6$ A/cm^2 at $T=77$ K and $H=0$ T). Films used in this work are c-axis oriented with thicknesses of 500 and 900 Å. Both films exhibit a linear dc resistivity above T_c and a sharp superconducting transition at 90 K with $\Delta T_c < 1$ K.

B. Terahertz system

Our terahertz experimental setup, based on the optoelectronic generation and reception of subpicosecond pulses of electromagnetic radiation, is similar to the one demonstrated originally by van Exter and Grischkowsky.[30] An optical beam from a self-mode-locked Ti:sapphire laser with pulses of 75–100 fs duration at a 76 MHz repetition rate is divided into pump (for exciting the transmitter) and probe (for gating the receiver) beams. The transmitter, biased with a dc voltage and triggered by the pump pulse, emits a short broadband electromagnetic burst generated from the photoconductive gap located in the center of a transmitting antenna.[31] The emitted radiation is collimated and illuminates the sample under study, and then the transmitted signal is focused on the receiver. The photocurrent from the receiver, corresponding to the radiated waveform in the time domain, is obtained using probe laser pulses that are synchronized and variably delayed with respect to the excitation (pump) pulses. The incident electric field is polarized parallel to the sample surface, and the transmitted, time-domain waveform is compared with that of a blank $LaAlO_3$ substrate mounted near the HTS film.

By performing a fast Fourier transform (FFT) of the temporal response data, both the field amplitude and phase transmitted through the thin-film–substrate composite in the frequency domain are obtained simultaneously without the need for a Kramers-Krönig analysis. When the film thickness, d, is smaller than the penetration depth and the wavelength, as in our case, the measured complex field transmission coefficient, γ, is related to the complex conductivity of the film, $\sigma(\omega)=\sigma_1(\omega)+i\sigma_2(\omega)$, by

$$\gamma = \Gamma e^{i\theta} = \frac{E_{\text{film/sub}}}{E_{\text{sub}}} = \frac{N+1}{N+1+Z_0 d\sigma}, \tag{1}$$

where E_{sub} and $E_{\text{film/sub}}$ are the induced electric fields on the receiver by the terahertz beam passed through the blank substrate and the thin-film–substrate, respectively, and $Z_0 = 377\Omega$ is the impedance of free space. The complex refractive index of the substrate, $N=n+ik$, was determined by measuring a blank $LaAlO_3$ reference. It was found that $n=4.85\pm0.03$, with very little dispersion, and $k/n \ll 0.01$ throughout the measured frequency range. Equation (1) takes into account multiple internal reflections in the thin film and neglects them in the substrate (where they appear outside the measurement time window). By solving Eq. (1) we find temperature and frequency dependent σ_1 and σ_2.

C. Femtosecond pump-probe spectroscopy

Femtosecond transient absorption spectroscopy at temperatures $T \approx 10$–300 K was performed using a standard pump-probe setup. The output beam with pulses of 75–100 fs from the self-mode-locked Ti:sapphire laser with a central wavelength of 780 nm (1.59 eV) were divided again into the pump and probe beams. The pump beam excited the carriers in the sample under study, and the probe beam measured the refractive index change produced by the pump beam by monitoring a time-dependent change in transmittance, ΔT, and/or reflectance, ΔR. The pump beam, chopped at 2 MHz by an acousto-optic modulator (for improving signal-to-noise-ratio), is focused normal to the sample surface to a 70-μm-diam spot size, while the probe beam is focused at about 5° incidence to a slightly smaller spot completely overlapped by the pump beam. The in-phase signals, ΔT and ΔR, associated with the probe beam were measured using a Si

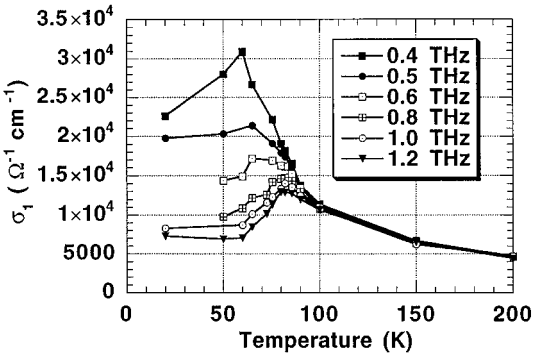

FIG. 1. Temperature dependence of the real part of σ_1 for the 900 Å sample at different THz frequencies reduced from the terahertz spectroscopy results.

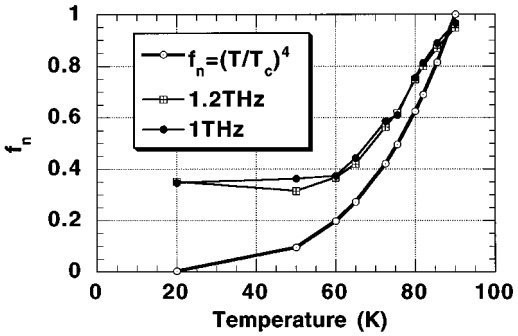

FIG. 2. Two-fluid Drude analysis of THz results: minimum values of normal fluid fraction, f_n, as a function of temperature at 1 and 1.2 THz compared with classical Gorter-Casimir values.

photodiode with a preamplifier and lock-in amplifier. The resolution of the measurements was better than $\Delta R/R \sim 10^{-6}$. To minimize the heating effects, the pump beam average power was limited to less than 10 mW and the probe beam average power was typically 10 times less than that of the pump beam.

III. CONDUCTIVITY PEAK FROM TERAHERTZ SPECTROSCOPY

A. Experimental results

Figure 1 shows the temperature dependence of the real part of the optical conductivity, σ_1, for the 900 Å sample reduced from the terahertz experimental data following the procedure described in Sec. II B. We can see a trend: development of a peak which increases in amplitude and moves to lower temperatures as we lower the frequency from 1.2 to 0.4 THz. The σ_1 peak shifts from about 82 K at 1.2 THz to about 62 K at 0.4 THz. Our results are consistent with the earlier reported terahertz results of Nuss *et al.*[8] in the frequency range between 0.5 and 2 THz where the σ_1 peak shifts from about 80 K at 2 THz to below 70 K at 0.5 THz. A similar trend was observed in microwave experiments at frequencies from 1 to 40 GHz but with the peak shifted to even lower temperatures (40–50 K).[6] We should note that a σ_1 peak in the frequency range between 1 and 1.2 THz in Fig. 1 has a small frequency dependence. This insensitivity to frequency may be due to the fact that BCS-like coherence effects should not be significant in this frequency range as we will show later in the text. Therefore, in the next section we will discuss the application of a two-fluid Drude model in this frequency range to interpret our results. Then in the following section we will further discuss the results presented in Fig. 1 using Mattis-Bardeen theory to account for the temperature-dependent shift in σ_1. Then we will discuss the role of BCS coherence factors to explain the controversy in σ_1 and $1/T_1$ data.

B. Application of two-fluid Drude model

The two-fluid Drude model has been frequently used in the analysis of HTS materials.[6,22] However, the applicability of this model to HTS at microwave and THz frequencies could be insufficient, especially in light of the fact that this model does not take into consideration BCS coherence effects. Indeed, this model cannot explain the strong frequency dependence of σ_1 presented in Fig. 1 below 1 THz as it is shown later in this section. Also the two-fluid Drude model does not give the exact solution for the quasiparticle relaxation time because of the fitting parameters required (e.g., plasma frequency or normal fluid density, etc.), and therefore, reduced data for the relaxation time could indicate only a certain range for the relaxation time rather than an exact value. Nevertheless, we attempt to use this model in the frequency range from 1 to 1.2 THz where σ_1 has only a small frequency dependence and presumably a small contribution from the BCS coherence factors.

We can write the real and imaginary parts of the frequency-dependent conductivity, $\sigma(\omega)=\sigma_1(\omega)+i\sigma_2(\omega)$, described by the two-fluid Drude model, as

$$\sigma_1(\omega)=\frac{f_n\omega_p^2\tau}{4\pi(1+\omega^2\tau^2)}, \tag{2}$$

$$\sigma_2(\omega)=\frac{f_n\omega_p^2\tau^2\omega}{1+\omega^2\tau^2}+\frac{f_s\omega_p^2}{4\pi\omega}, \tag{3}$$

where f_n and f_s are the normal and superconducting fluid fractions ($f_n+f_s=1$), ω_p is a plasma frequency, and τ is a quasiparticle relaxation time.

Our goal is to extract f_n and τ from the experimental data (σ_1 and σ_2). However, we have three unknowns (τ, ω_p, and f_n) and only two equations, which is not adequate to find the exact solution. We describe the detailed procedure for careful reduction of f_n and τ in the Appendix.

Since the BCS coherence factors are not included in the two-fluid Drude model, we use terahertz frequencies between 1 and 1.2 THz where, as we stated above, BCS coherence effects should be insignificant. Figure 2 shows the temperature dependence of the minimum values of f_n from Eq. (A4) (see the Appendix) at 1 and 1.2 THz along with calculated classical Gorter-Casimir (GC) values using Eq. (A5). It is evident from Fig. 2 that the minimum values of f_n below T_c (90 K) are much higher than the GC values. This is an important observation which leads us to the idea that the superconducting energy gap may have a slower rate of increase below T_c than would be expected from the classical BCS behavior. Indeed, a higher normal fluid concentration should lower the energy gap, because, conversely, a smaller energy gap increases the probability of breaking Cooper

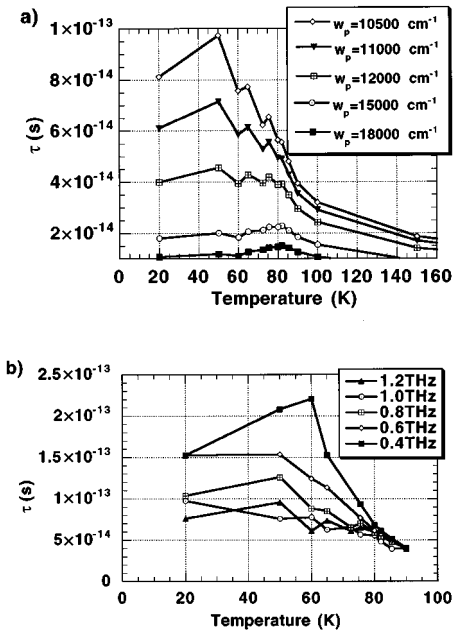

FIG. 3. Quasiparticle relaxation time reduced from two-fluid Drude model: (a) at 1 THz for variable fitting parameter ω_p; (b) at $\omega_p = 10\,500$ cm^{-1} at different THz frequencies.

pairs by phonons, thus increasing the number of quasiparticles. This could possibly be caused by an anisotropic nature (e.g., *d* wave or *s* wave) of the gap, and we will address this later in the paper.

Figure 3(a) shows the temperature dependence of the relaxation time at 1 THz for a range of plasma frequencies from 10500 to 18000 cm^{-1} calculated using Eq. (A6) (results for 1.2 THz are similar). The low limit for plasma frequencies is determined by the condition described by Eqs. (A4), (A1), and (A2). The common feature for all these curves is a relatively mild increase in relaxation time (e.g., from 30 fs at 90 K to 60 fs at 60 K for a plasma frequency of 11 000 cm^{-1}) below T_c. This change in relaxation rate may have a contribution to the peaks in σ_1 shown in Fig. 1 (especially, in the frequency range between 1 and 1.2 THz) as a result of competition between reducing relaxation rate and decreasing normal fluid density. The same arguments were made by Nuss *et al.*[8] for the THz case and by Bonn *et al.*[6] for the microwave case. However, application of the two-fluid model and, therefore, these arguments fail to account for the fact that σ_1 increases in amplitude and the peak moves to lower temperature as we decrease the frequency (see the significant change in σ_1 in the frequency range from 1 to 0.4 THz in Fig. 1). Indeed, this model cannot explain a strong frequency dependence of σ_1 presented in Fig. 1 below 1 THz because it leads to the ambiguity in data reduction for the quasiparticle relaxation time, i.e., a significant difference (more than 100%) in the relaxation time reduced from the two-fluid model using the procedure outlined in this paper for the frequency range between 1 and 0.4 THz as shown in Fig. 3(b). Therefore, we believe that some BCS-like coherence factors make an important contribution which explains such a strong frequency dependence of σ_1. This is addressed next.

C. Fitting the conductivity with Mattis-Bardeen theory

It was pointed out above that the two-fluid Drude model cannot adequately explain the fact that the peak in σ_1 increases in amplitude and moves to lower temperatures as the frequency decreases in Fig. 1. Therefore, we believe that some BCS-like coherence factors could play an important role in explaining such a strong dependence of σ_1 on frequency. The obvious difficulty is that there is no consensus on the mechanism of high-T_c superconductivity. Another difficulty is a material factor: results reported on different samples by different groups vary (i.e., the position and amplitude of the conductivity peak).[6–10] Nevertheless, to model our conductivity data, we have used the BCS-based Mattis-Bardeen theory[32] with expressions for the superconducting conductivity normalized to the normal conductivity (in a dirty limit) given by

$$\frac{\sigma_1}{\sigma_n} = \frac{2}{\hbar\omega}\int_{\Delta}^{\infty}[f(E)-f(E+\hbar\omega)]g(E)dE + \frac{1}{\hbar\omega}\int_{\Delta-\hbar\omega}^{-\Delta}[f(E)-2f(E+\hbar\omega)]g(E)dE, \quad (4)$$

$$\frac{\sigma_2}{\sigma_n} = \frac{1}{\hbar\omega}\times\int_{\Delta-\hbar\omega,-\Delta}^{\Delta}\left(\frac{[1-2f(E+\hbar\omega)](E^2+\Delta^2+\hbar\omega E)dE}{\sqrt{(\Delta^2-E^2)[(E+\hbar\omega)^2-\Delta^2]}}\right), \quad (5)$$

where Δ is the superconducting energy gap, $f(E)=(e^{E/k_BT}+1)^{-1}$ is the usual Fermi-Dirac function, $\varepsilon_1=\sqrt{E^2-\Delta^2}$ and $\varepsilon_2=\sqrt{(E+\hbar\omega)^2-\Delta^2}$ are the Bloch energies corresponding to energies E and $E+\omega\hbar$, respectively, and $g(E)=(E^2+\Delta^2+\hbar\omega E)/\varepsilon_1\varepsilon_2$.

We have also used an expanded version of the Mattis-Bardeen theory,[33–35] which includes the quasiparticle scattering rate, to model optical conductivity for our data. The expression for $\sigma(\omega)$ normalized to the normal dc conductivity, σ_0, is (with $\hbar=1$) (Ref. 33)

$$\frac{\sigma(\omega)}{\sigma_0} = \frac{i}{2\omega\tau}\left(J+\int_{\Delta}^{\infty}I_2dE\right), \quad (6)$$

where

$$J(\omega\leqslant 2\Delta) = \int_{\Delta}^{\omega+\Delta} I_1 dE,$$

$$J(\omega\geqslant 2\Delta) = \int_{\Delta}^{\omega-\Delta} I_3 dE + \int_{\omega-\Delta}^{\omega+\Delta} I_1 dE,$$

$$I_1=\tanh\frac{E}{2kT}\left\{\left[1-\frac{\Delta^2+E(E-\omega)}{P_4P_2}\right]\frac{1}{P_4+P_2+i/\tau}-\left[1+\frac{\Delta^2+E(E-\omega)}{P_4P_2}\right]\frac{1}{P_4-P_2+i/\tau}\right\},$$

$$I_2=\tanh\frac{E+\omega}{2kT}\left\{\left[1+\frac{\Delta^2+E(E+\omega)}{P_1P_2}\right]\frac{1}{P_1-P_2+i/\tau}-\left[1-\frac{\Delta^2+E(E+\omega)}{P_1P_2}\right]\frac{1}{-P_1-P_2+i/\tau}\right\}$$
$$+\tanh\frac{E}{2kT}\left\{\left[1-\frac{\Delta^2+E(E+\omega)}{P_1P_2}\right]\frac{1}{P_1+P_2+i/\tau}-\left[1+\frac{\Delta^2+E(E+\omega)}{P_1P_2}\right]\frac{1}{P_1-P_2+i/\tau}\right\},$$

$$I_3=\tanh\frac{E}{2kT}\left\{\left[1-\frac{\Delta^2+E(E-\omega)}{P_3P_2}\right]\frac{1}{P_3+P_2+i/\tau}-\left[1+\frac{\Delta^2+E(E-\omega)}{P_3P_2}\right]\frac{1}{P_3-P_2+i/\tau}\right\},$$

$$P_1=\sqrt{(E+\omega)^2-\Delta^2},\qquad P_2=\sqrt{E^2-\Delta^2},$$

$$P_3=\sqrt{(E-\omega)^2-\Delta^2},\quad P_4=i\sqrt{\Delta^2-(E-\omega)^2}.$$

This expression applies to isotropic BCS superconductors with a spherical Fermi surface; its extension to superconductors with an anisotropic gap or to the presence of several gaps may be simply achieved by linear superposition.[33] In this simulation we have used the range for relaxation time corresponding to the two-fluid model results [Fig. 3(a)]: $1/\tau$=80–500 cm^{-1} (9.4×10^{13} s^{-1} to 1.5×10^{13} s^{-1}, respectively). We have found that the variation in $1/\tau$ in this range did not have an appreciable effect on the results. We also assume the films have an anisotropic energy gap, which implies the averaging of the conductivity tensor in the a-b plane (thus the average anisotropic gap may be considered in our simulations). Two parameters have then been varied: the energy gap at 0 K and the temperature dependence of the energy gap. Following our pump-probe spectroscopy results which will be presented in the next section, as well as our observations from the two-fluid Drude model interpretation of the THz results, we have used a gap which opens up more slowly below T_c than the classical BCS gap. Therefore, in our simulation we have used the temperature-dependent gap described by a general expression with variable parameter n:

$$\Delta(T)\sim\left(1-\frac{T}{T_c}\right)^n. \tag{7}$$

Figure 4 shows examples of fitting σ_1 with Mattis-Bardeen theory using an algorithm described by Eq. (6) [simulation results in the BCS classical dirty limit using Eq. (4) are similar to those shown in Fig. 4]. Glassical BCS behavior, with zero-temperature gap, $2\Delta(0)$=225 cm^{-1} (27.9 meV), is shown in Figs. 4(a). Figures 4(b) and 4(c) show an example of σ_1 simulation for different frequency ranges [from 10^{-3} to 1.2 THz in Figs. 4(c) and from 0.1 to 1.2 THz in Fig. 4c] using a zero-temperature gap of 225 cm^{-1} corresponding to BCS weak coupling, and Eq. 7 with n=0.9 for the slower than BCS temperature-dependent gap increase below T_c (the choice of n for this simulation is justified by the results presented in the next section). The BCS simulation in Fig. 4(a) shows a peak developing and increasing in amplitude when the frequency is decreased from 1 to 0.001 THz. [Note that, since the σ_1 calculation using Eq. (6) involves integration around singularity points, the amplitude of peaks in this simulation could be varied, which makes the location of the peaks more important than their amplitude.] However, this peak has a small temperature dependence (shifting from 85 to 76 K) which is inconsistent with the conductivity data shown in Fig. 1. The simulation shown in Figs. 4(c) and 4(b) is a much closer fit to our data shown in Fig. 1: the σ_1 peak increases in amplitude and shifts to about 62 K at 0.4 THz. This peak shifts even further to 53 K at 0.001 THz. Note that by varying the temperature-dependent gap [e.g., changing n in Eq. (7)] and zero-temperature gap, the σ_1 peak could be shifted to even lower temperatures to account for variation of results reported by different groups.[6,8]

To further interpret the experimental results we compare our simulations with the experimental conductivity data shown in Fig. 1. Figure 5 shows the temperature peak ($T_{\rm peak}$) dependence of σ_1 as a function of frequency for the two simulation cases (the BCS gap, and the gap described by Eq. (7) with n=0.9) and for the conductivity data of Fig. 1. It is clearly seen that, in the simulation case with the classical BCS gap, $T_{\rm peak}$ frequency dependence is significantly different from our experimental data. On the contrary, for the second case with the gap described by Eq. (7) with n=0.9, $T_{\rm peak}$ follows rather closely the experimental results in the frequency range between 0.2 and 0.5 THz. Above 0.5 THz the difference between the simulation and experimental data starts to develop and quickly increase. Also, note that $T_{\rm peak}$ for the experimental conductivity data stays constant at 82 K for the frequencies above 0.8 THz.

We would like to propose the following qualitative explanation to the observed phenomena. The mild peak in σ_1 at about 82 K for the frequency range between 1 and 1.2 THz in Fig. 1 could be caused by the competition between the drop in scattering rate and the decreasing normal fluid density with temperature. This peak is relatively small and frequency independent. However, when we decrease frequency below 1 THz the BCS-like coherence peak [simulation is shown in Figs. 4(b) and 4(c)] starts to develop, gradually increasing its contribution to σ_1. As the frequency is decreased from 1 to 0.8 THz, the coherence factors contribution is still insignificant which only results in a slight increase of the σ_1 peak in Fig. 1 without a noticeable shift in $T_{\rm peak}$ in Fig. 5. However, as the frequency is decreased below

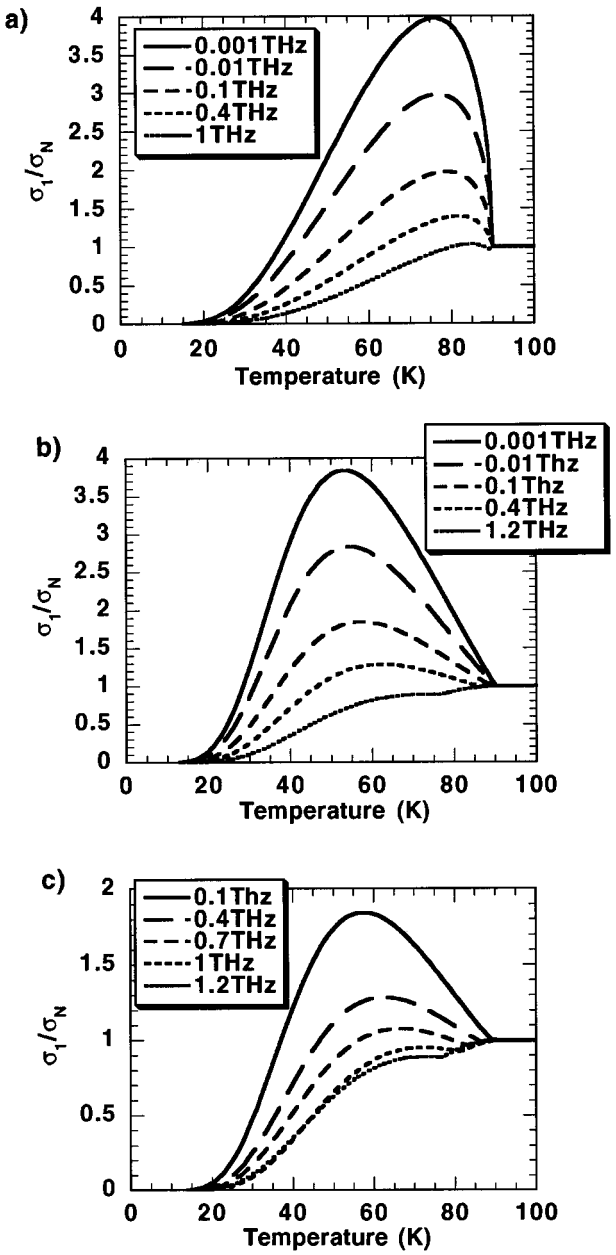

FIG. 4. Fitting σ_1 with Mattis-Bardeen theory including scattering rate ($1/\tau$=500 cm^{-1}): (a) for the classical BCS gap; (b) and (c) for different frequency ranges using identical parameters: $\Delta(T)\sim(1-T/T_c)^{0.9}$ and $2\Delta(0)$=225 cm^{-1}.

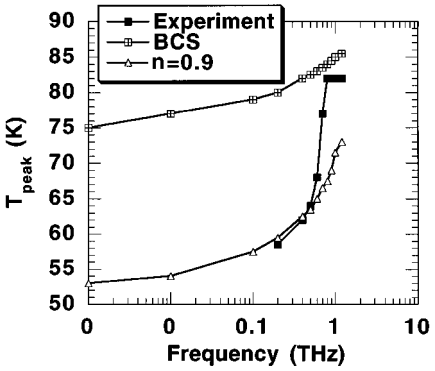

FIG. 5. Temperature peak (T_{peak}) dependence of σ_1 as a function of frequency for the two simulation cases [the BCS gap and the gap described by Eq. (7) with n=0.9] and for the experimental conductivity data of Fig. 1.

0.8 THz, the contribution of coherence factors increases further to the extent that the σ_1 peak due to these factors starts to dominate. This significantly shifts T_{peak} in Fig. 5 and increases the σ_1 peak in Fig. 1. As we pointed out above, the T_{peak} frequency dependence in Fig. 5 for the simulation, shown in Figs. 4(b) and 4(c) follows rather closely the experimental results in the frequency range between 0.2 and 0.5 THz, which is most likely due to the total domination of the contribution from the coherence factors.

Thus, we have come to the conclusions that the development of the frequency-dependent peak in σ_1 can be fitted by the BCS-based Mattis-Bardeen theory of conductivity using an energy gap approximated by Eq. (7). Next we will discuss the role of BCS coherence factors to explain the controversy in σ_1 and $1/T_1$ data.

D. Discussion of coherence factors in σ_1 and $1/T_1$

We discuss the role of coherence factors to account for the presence of the conductivity peak and the absence of the peak in NMR relaxation-rate data. The coherence factors are given by[36]

$$l^2(\varepsilon_k,\varepsilon_{k+q})=\frac{1}{2}\left(1+\frac{\varepsilon_k\varepsilon_{k+q}+\Delta_k\Delta_{k+q}}{E_kE_{k+q}}\right), \tag{8}$$

$$p^2(\varepsilon_k,\varepsilon_{k+q})=\frac{1}{2}\left(1-\frac{\varepsilon_k\varepsilon_{k+q}+\Delta_k\Delta_{k+q}}{E_kE_{k+q}}\right), \tag{9}$$

where $E_k=\sqrt{\varepsilon_k^2+\Delta_k^2}$, $E_{k+q}=\sqrt{\varepsilon_{k+q}^2+\Delta_{k+q}^2}$, $\mathbf{k}$ and $\mathbf{k}'=\mathbf{k}+\mathbf{q}$ are quasiparticle wave vectors, ε_k and ε_{k+q} are quasiparticle initial and final Bloch energies relative to the Fermi level, and Δ_k and Δ_{k+q} are the corresponding superconducting energy gap parameters.

BCS Mattis-Bardeen conductivity expressions given by Eqs. (4) and (5) as well as expressions for NMR relaxation rate, $1/T_1$, exhibiting coherence peaks, are derived by neglecting crystalline anisotropy (using an isotropic limit) of the superconducting material. This condition implies that in coherence factors described by Eqs. (8) and (9) for any direction in $\mathbf{k}$ space, the following should be valid:

$$\Delta_k=\Delta_{k+q}. \tag{10}$$

However, HTS are highly anisotropic materials, therefore, Eq. (10) should be evaluated for these cases.

For the electromagnetic absorption case and, particularly, for the THz results presented in this paper, we consider a ''long-wavelength limit,'' i.e., $\mathbf{q}\to 0$, because, indeed, the photon wave vector, $\mathbf{q}$, is very small (less than 100 cm^{-1} for THz excitation) compared to the wave vector of the electrons $\mathbf{k}$ ($\sim 10^8$ cm^{-1}). Thus, in spite of the anisotropy of the superconducting energy gap in $\mathbf{k}$ space, $\mathbf{k}\approx\mathbf{k}+\mathbf{q}$, and, therefore,

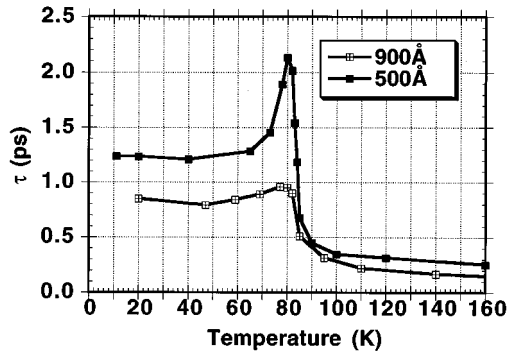

FIG. 6. Relaxation time (at half maximum) as a function of temperature for the 500 and 900 Å samples measured by the femtosecond pump-probe spectroscopy.

Eq. (10) is valid for the electromagnetic absorption case, and Mattis-Bardeen theory is applicable for HTS.

The situation is different for the NMR relaxation case. Quasiparticles scatter in **k** space through electron-phonon and electron-electron scattering, and in general $\mathbf{k}+\mathbf{q}\neq\mathbf{k}$. This means that for the anisotropic HTS Eq. (10) in not valid. This suppresses the role of the coherence factors [described by Eqs. (8) and (9)] for the NMR relaxation, which explains the absence of the peak in NMR relaxation rate. This is the fundamental difference between the coherence factors to account for σ_1 and $1/T_1$ HTS experimental data. Lu[24] went even further in finding evidence of coherence factors based on the change of the anisotropic ratio of scattering rates in the a and c directions (W_{1a}/W_{1c}). Simple arguments presented above can explain and reconcile the controversy related to the role of coherence factors in σ_1 and $1/T_1$ data for HTS.

IV. RELAXATION TIME FROM PUMP-PROBE FEMTOSECOND SPECTROSCOPY

A. Results and discussions

Figure 6 shows the temperature dependence of the relaxation time measured by the femtosecond pump/probe spectroscopy for the 900 and 500 Å samples. The relaxation time has an enhancement below T_c and a peak near T_c. These results are well established and similar to those reported in the literature.[17–21] A discussion of the mechanism of the nonequilibrium optical response of high-T_c superconductors has been presented by Frenkel,[37] and the reader can find important details in this reference to better understand the following arguments. However, for the completeness of this paper and for the convenience of the reader, we repeat here the main relevant points.

We use the BCS description of a superconductor in this model. The condensate (Cooper pairs) exchanges energy with quasiparticles (unpaired electrons above the energy gap) through pair breaking and recombination via phonons (electron-phonon scattering) and via quasiparticles (electron-electron scattering). The quasiparticle energy spectrum (or spectral density), $f_0(E)$, is in equilibrium, which is maintained (in addition to exchange with the condensate) by electron-phonon scattering (exchange with phonons), by electron-electron scattering, and by diffusion. Phonons participate in electron-phonon and phonon-phonon interactions [the phonon equilibrium energy spectrum, $F_0(\Omega)$]. Phonon equilibrium is maintained by their escape to the thermal bath.

A femtosecond optical pulse creates a nonequilibrium condition in the superconductor by exciting quasiparticles and breaking Cooper pairs. As a result, the spectrum of quasiparticles is instantaneously changed, creating a highly nonequilibrium situation where the electron temperature could significantly exceed the phonon temperature. The quasiparticle time-dependent energy spectrum $f(E,t)$, where E is the quasiparticle energy and t is the time, is determined by a rather complex exchange of electrons and phonons, governed by electron-phonon and electron-electron scattering (quasiparticle interactions with themselves, the condensate, and phonons). As a result of electron-phonon scattering, extra phonons of high energy (optical phonons) with the spectrum $\Delta F(\Omega,t)$ are generated.

The rate of phonon and electron escape to the thermal bath determines in many respects the nonequilibrium dynamics of the optical response, since these extra phonons and electrons continue to cause nonequilibrium transitions. Therefore, in the framework of nonequilibrium superconductivity, the relaxation of the phonon and electron spectra to the equilibrium values becomes a bottleneck of the relaxation process. Since the superconducting gap is in turn disturbed by the nonequilibrium values of the phonon and electron spectra (or temperatures), the relaxation of the energy gap to its equilibrium value becomes a bottleneck for the quasiparticle relaxation process. This allows us to model relaxation time by the change in the energy gap created by a femtosecond optical pulse. We will describe this model in the next section. Before that we examine our pump-probe results in conjunction with the terahertz spectroscopy results.

First, we see that the relaxation time at terahertz frequencies (Fig. 3) has a weaker enhancement below T_c in comparison with the pump-probe data (Fig. 6). We expect this because at terahertz frequencies (1 THz corresponds to a photon energy of 4 meV) there should be no excitation (i.e., breaking of Cooper pairs) over the superconducting energy gap (BCS zero-temperature gap is 28 meV) by the terahertz photons directly. Therefore, interaction with Cooper pairs is insignificant in this case, and it is mainly due to a small thermal disturbance of the energy gap caused by the nanowatt terahertz beam. There is a possibility that because of the slow opening of the energy gap below T_c, the increase in the relaxation time near T_c in the case of the THz excitation may also be due to the breaking of Cooper pairs with a subsequent slow recombination process of quasiparticles to Cooper pairs. However, this effect in the THz case is much weaker than that for the pump-probe high-energy excitation (1.59 eV). Therefore, the recombination of quasiparticles to Cooper pairs and energy gap disturbance have a less significant effect in the terahertz case, which may explain the lack of a dramatic enhancement of relaxation time in this experiment as compared to the pump/probe measurement, where the energy gap disturbance and recombination of quasiparticles to Cooper pairs are slowing factors.

Another difference between the terahertz and pump-probe experiments is the order of magnitude of the relaxation time. The reason for this can be explained as follows. Quasiparti-

cle excess energy for the pump-probe excitation with photon energy of 1.59 eV is almost 3 orders of magnitude larger than for THz excitation. Thus, no matter what the quasiparticle relaxation mechanism (electron-phonon or electron-electron scattering) there may be significantly more steps in the quasiparticle relaxation process for pump-probe excitation. This multistep process, relaxation of the energy gap, as well as possibly a slow recombination process of quasiparticles to Cooper pairs, make quasiparticle relaxation in the pump-probe experiment approximately 1–2 orders of magnitude slower than for THz excitation below T_c. Above T_c one should expect that the pump-probe relaxation will be faster because of the elimination of the energy gap relaxation and recombination of quasiparticles to Cooper pairs. This phenomena can be seen in Fig. 6. However, since we reach the time-resolution limit of the pump-probe measurements above T_c, the results in Fig. 6 are inconclusive for a direct comparison of the pump-probe and THz relaxation process data above T_c.

B. Model for relaxation time

There are two important factors contributing to the enhancement of the relaxation time below T_c: the opening of the energy gap and its perturbation by the excitation pulse. Thus, in the framework of nonequilibrium superconductivity, the quasiparticle spectrum excited by the laser pulse relaxes to the ''equilibrium'' determined by the instantaneous value of the energy gap, and therefore, relaxation of the energy gap becomes a bottleneck in the quasiparticle relaxation process. Indeed, before the energy gap relaxes to its initial equilibrium, Cooper pairs could be broken by the lower energy phonons, maintaining nonequilibrium in quasiparticle spectrum. Thus, the larger the change in the energy gap caused by the excitation pulse, the more steps in the relaxation and recombination process are required to return to the initial equilibrium, resulting in an increased relaxation time.

In that regard we use a simple model to explain our data shown in Fig. 6. We assume that the pump pulse, absorbed via electron transitions, ''heats'' the sample, which results in the energy gap changing by a certain amount proportional to the intensity of the laser pulse. This is supported by the early data of Han *et al.*,[18] where they show that the peak in the relaxation time is shifted towards T_c at lower intensity. Since the relaxation time peak in our data is at ~80 K and T_c=90 K we assume that the pump pulse causes about a 10 K increase in lattice temperature, completely destroying the energy gap at 80 K. We estimate the maximum lattice temperature rise, ΔT, in the superconducting film caused by the femtosecond pulse using a simplified method outlined by Frenkel *et al.*[37,38] based on heat transfer equations[39] as follows:

$$\Delta T = \frac{1.12E}{A\sqrt{\Delta t k c \rho}}, \tag{11}$$

where E is the laser pulse energy absorbed by the HTS film, A is the pump beam area on the film, Δt is the laser pulse width, and k, c, and ρ are the thermal conductivity, specific heat, and density of $LaAlO_3$. We have calculated ΔT from Eq. (11) to be in the range 7.2–11.9 K using the following parameters: E=0.033–0.045 nJ, Δt=75–100 fs, $A=0.4\times10^{-4}$ cm^2, k=0.26 W/cm K at 80 K,[40] c=0.09 J/g K,[41] and ρ=6.52 g/cm^3.[42] This estimate is close to our assumption of a 10 K rise in lattice temperature. We thus consider the change in the energy gap equivalent to the 10 K lattice heating without arguing what exactly causes the change in the gap: lattice heating or some other nonequilibrium factors. Then the model for simulation is straightforward. We assume for simplicity that the relaxation time, τ, is proportional to the change in the energy gap, $\delta\Delta(T)$, caused by the pump pulse:

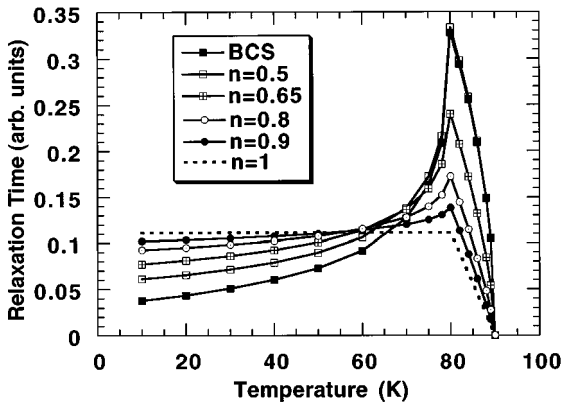

FIG. 7. Simulation of the relaxation time in the pump-probe experiment by the change in the superconducting energy gap for different temperature-dependent gaps: BCS gap and the gap described by Eq. (6) with different n.

$$\tau \sim \delta\Delta(T) \sim \Delta(T) - \Delta(T+dT), \tag{12}$$

where dT is the equivalent temperature increase caused by the excitation pulse. Then, considering the superconducting gap in the form described by Eq. (7), we can easily show that

$$\tau \sim \delta\Delta(T) \sim \left(1-\frac{T}{T_c}\right)^n - \left(1-\frac{T+dT}{T_c}\right)^n \quad \text{for } T<T_c-dT, \tag{13}$$

$$\tau \sim \delta\Delta(T) \sim \left(1-\frac{T}{T_c}\right)^n \quad \text{for } T_c>T>T_c-dT. \tag{14}$$

The results of τ simulation using Eqs. (13) and (14) with dT=10 K and T_c=90 K for different n in Eq. (7) are shown in Fig. 7. Comparing Figs. 6 and 7 we can see that the best fitting parameter for the 900 Å sample is about n=0.9. For the 500 Å sample the best fit is achieved with n~0.75. However, at low temperatures (below 40 K) the relaxation time shown in Fig. 7 is decreasing, whereas it is increasing below 40 K in our experimental data shown in Fig. 6. Therefore, we believe that other factors (e.g., increase in the recombination time of quasiparticles to Cooper pairs) start to make an important contribution to a mild increase in τ below 40 K shown in Fig. 6. This means that our model for the relaxation time described above (relaxation time is proportional to the change in the energy gap) may not be applied for the temperatures below 40 K. Therefore, the energy gap behavior below 40 K (or approximately below $T_c/2$) is inconclusive from our data and modeling.

We also want to mention that other factors can contribute to the enhancement of the quasiparticle relaxation time in the pump-probe experiment. For example, the recombination time of quasiparticles to Cooper pairs can also be a ''slow'' process, contributing to the relaxation time enhancement (especially at low temperatures as described above). Another factor could be related to the changes in thermal conductivity below T_c,[43] which may change the quasiparticle mean free path and, therefore, effect the quasiparticle scattering time. However, we believe that these factors do not have a strong enough temperature dependence to support the data in Fig. 6 and, therefore, are secondary compared to the changes in the energy gap which are described here, especially near T_c.

C. Discussion of energy gap

The important conclusion from the results presented above is the fact that the superconducting gap in our films could be approximated by Eq. (7) with the parameter n between 0.75 and 0.9 (close to 0.9 for 900 Å sample). This means that the superconducting gap opens up substantially slower below T_c than expected for a classical BCS superconductor. One can question how universal this conclusion is, and is it an attribute of our films or intrinsic properties of high-T_c materials in general? That is yet to be seen. As an illustration we would like to compare our results with recent theoretical work[23,44] which supports our findings (slower energy gap change below T_c) in the frame of an anisotropic s-wave gap based on the Anderson theory of interlayer tunneling.[45] Figure 8 compares calculations of the minimum gap from this reference [Fig. 8(b)] (Ref. 45) with the simulation of the gap by BCS fitting and by Eq. (7) with different n [Fig. 8(a)]. There is a good agreement between these two interpretations of energy gap, especially in the temperature range from $T_c/2$ to T_c. However, we would like to make clear that our results do not suggest that the gap is s wave, d wave, or otherwise. It simply indicates that the anisotropic energy gap in average opens up more slowly than a BCS gap below T_c. Therefore, if this conclusion is correct, then any HTS theory should account for this finding. Finally, in our simulation we have used the gap described by Eq. (7) as one example of a gap dependence which varies slowly with temperature below T_c. We will continue looking for various anisotropic temperature dependent gaps (e.g., anisotropic s-wave gap,[23,44] d wave etc.) to fit our σ_1 data.

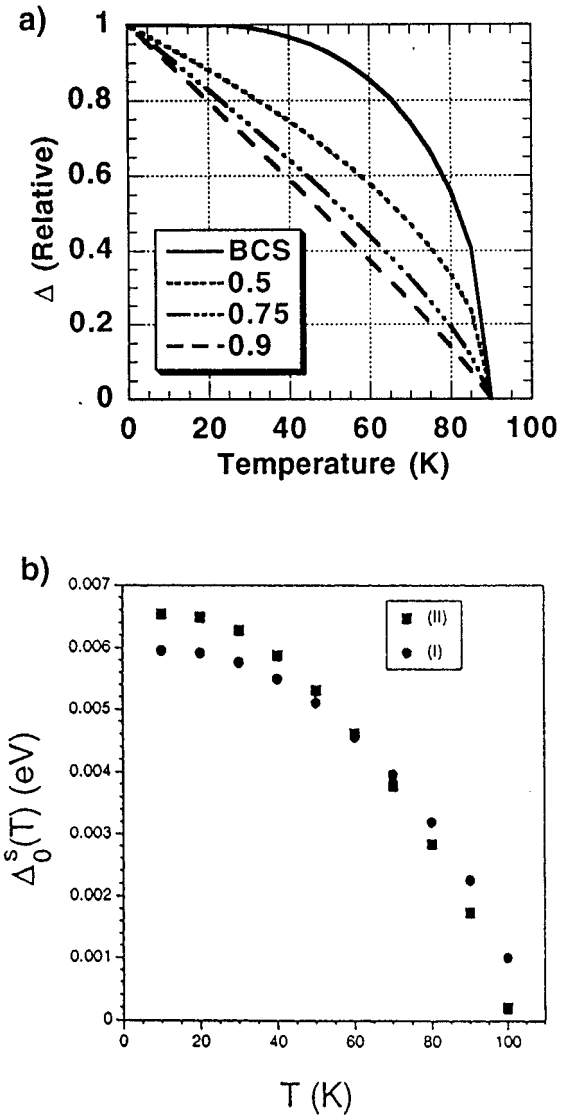

FIG. 8. Comparison of superconducting energy gap: (a) simulation of a temperature-dependent gap by $\Delta(T)\sim(1-T/T_c)^n$ with different n; the BCS gap is shown for comparison; (b) minimum anisotropic s-wave gap values from Sudbø *et al.* (Ref. 23); circles and squares in (b) represent gaps calculated in Ref. 23 with different fitting parameters.

V. CONCLUSION

In this paper we clarify the origin of the coherent peak in σ_1 in relationship to the BCS coherent factors, to the temperature dependence of the energy gap, and to the quasiparticle relaxation rate. We showed that σ_1 reduced from our terahertz spectroscopy measurements performed on high-quality, single-crystal YBCO thin films (900 and 500 Å) has a ''coherence'' peak which increased in amplitude and shifted to lower temperatures as we change frequency from 1.2 to 0.4 THz. Although the quasiparticle relaxation time reduced from these results using the two-fluid Drude model exhibits an enhancement below T_c, the analysis may not be adequate to account for the strong frequency dependence of the conductivity peak. That is, the competition between the drop in scattering rate and the decreasing normal fluid density with temperature may not sufficiently explain the peak in σ_1.

On the contrary, we were able to fit σ_1 by Mattis-Bardeen theory using a BCS gap which opened more slowly below T_c than that of a typical BCS superconductor. This is consistent with the higher normal fluid density (higher than the Gorter-Casimir values) obtained from the two-fluid Drude model interpretation of our THz data. Therefore, our results suggest that an anisotropic energy gap which in average increases relatively slowly below T_c is responsible for the ''modification'' (shifting to lower temperatures) of the coherence peak in σ_1. Furthermore, we have discussed the role of coherent factors to account for the presence of the conductivity peak and the absence of the peak in NMR relaxation rate. We have concluded that our THz spectroscopy results are consistent

with the presence of coherence factors in an anisotropic superconductor.

Furthermore, we present a model for the quasiparticle relaxation time measured by femtosecond pump-probe spectroscopy, where this relaxation time is proportional to the change in the energy gap imposed by the femtosecond pulse. This model allowed us to find a fit to the temperature-dependent energy gap function which is also consistent with the slower gap increase below T_c. The latest theoretical developments based on an anisotropic, *s*-wave, BCS-like gap[23] coincide with our conclusion about a more slowly opening gap below T_c.

ACKNOWLEDGMENTS

We would like to thank Philip Anderson and Steven Strong for valuable discussions. Work at the University of Michigan was supported by the National Science Foundation through the Center for Ultrafast Optical Science under STC PHY 8920108.

APPENDIX: DATA REDUCTION USING TWO-FLUID DRUDE MODEL

The real and imaginary parts of the frequency-dependent conductivity, $\sigma(\omega)$, described by the two-fluid Drude model are given by Eqs. (2) and (3). The values of f_n and τ can be extracted from the experimental data (σ_1 and σ_2). However, we have three unknowns (τ, ω_p, and f_n) and only the two equations, which do not give us a direct solution. Therefore the analysis proceeds as follows.

Step 1: Assume f_n is known, then solve Eqs. (2) and (3) to find τ and ω_p as

$$\tau=\frac{Af_n\pm\sqrt{A^2f_n^2-4(1-f_n)}}{2\omega}, \tag{A1}$$

$$\omega_p=\sqrt{\frac{\sigma_1 4\pi(1+\omega^2\tau^2)}{f_n\tau}}, \tag{A2}$$

where $A=\sigma_1/\sigma_2$.

In order for τ to be real, we have to request [from Eq. (A1)] that

$$A^2f_n^2-4(1-f_n)\geqslant 0. \tag{A3}$$

The solution of Eq. (A3) is straightforward (we take positive f_n):

$$f_n\geqslant\frac{2(\sqrt{1+A^2}-1)}{A^2}. \tag{A4}$$

Step 2: Compare the minimum value of f_n from Eq. (A4) (equality case) with the well-known Gorter-Casimir expression:[46]

$$f_n=\left(\frac{T}{T_c}\right)^4. \tag{A5}$$

Figure 2(a) shows the temperature dependence of the minimum values of f_n from Eq. (A4) (explanations are given in the text).

Step 3: Assume ω_p is known, then solve Eqs. (2) and (3) for τ and f_n:

$$\tau=\frac{\sigma_1 4\pi}{\omega_p^2-\sigma_2 4\pi\omega}, \tag{A6}$$

$$f_n=\frac{\sigma_1 4\pi(1+\omega^2\tau^2)}{\omega_p^2\tau}. \tag{A7}$$

Figure 3 shows the temperature dependence of the relaxation time for different values of ω and ω_p calculated from Eq. (A6) (explanations are given in the text). The range of plasma frequencies is determined from Eqs. (A4), (A1), and (A2).

*Present address: School of Mathematical Science and Engineering, New Mexico Highlands University, Las Vegas, New Mexico 87701.

†Present address: University of Illinois at Urbana-Champaign, Department of Physics and Materials Research Laboratory, Urbana, IL.

‡Present address: Sandia National Laboratory, Albuquerque, NM 87185.

[1] J. Bardeen, L. N. Cooper, and J. R. Schrieffer, Phys. Rev. **108**, 1175 (1957).

[2] L. H. Palmer and M. Tinkham, Phys. Rev. **165**, 588 (1968).

[3] J. Bardeen and J. R. Schrieffer, *Progress in Low Temperature Physics* (North-Holland, Amsterdam, 1961), Vol. III.

[4] L. C. Hebel and C. P. Slichter, Phys. Rev. **107**, 901 (1957); **113**, 1504 (1959).

[5] A. G. Redfield and A. G. Anderson, Phys. Rev. **116**, 583 (1959); A. G. Redfield, Phys. Rev. Lett. **3**, 85 (1959); Y. Masuda and A. G. Redfield, Phys. Rev. **125**, 159 (1962).

[6] D. A. Bonn, P. Dosanjh, R. Liang, and W. N. Hardy, Phys. Rev. Lett. **68**, 2390 (1992); D. A. Bonn, R. Liang, T. M. Riseman, D. J. Baar, D. C. Morgan, K. Zhang, P. Dosanjh, T. L. Duty, A. MacFarlane, G. D. Morris, J. H. Brewer, W. N. Hardy, C. Kallin, and A. J. Berlinsky, Phys. Rev. B **47**, 11314 (1993); D. A. Bonn, S. Kamal, K. Zhang, R. Liang, D. J. Baar, E. Klein, and W. N. Hardy, *ibid*. **50**, 4051 (1994); Kuan Zhang, D. A. Bonn, S. Kamal, R. Liang, D. J. Baar, W. N. Hardy, D. Basov, and T. Timusk, Phys. Rev. Lett. **73**, 2484 (1994).

[7] F. Gao, J. W. Kruse, C. E. Platt, M. Feng, and M. V. Klein, Appl. Phys. Lett. **63**, 2274 (1993).

[8] M. C. Nuss, P. M. Mankiewich. M. L. O'Malley, E. H. Westerwick, and P. B. Littlewood, Phys. Rev. Lett. **66**, 3305 (1991).

[9] K. Holczer, L. Forro, L. Mihály, and G. Grüner, Phys. Rev. Lett. **67**, 152 (1991).

[10] D. B. Romero, C. D. Porter, D. B. Tanner, L. Forro, D. Mandrus, L. Mihály, G. L. Carr, and G. P. Williams, Phys. Rev. Lett. **68**, 1590 (1992).

[11] S. E. Barrett, J. A. Martindale, C. P. Slichter, T. A. Friedmann, J. P. Rice, and D. M. Ginsberg, Phys. Rev. Lett. **66**, 108 (1991); J. A. Martindale, S. E. Barrett, C. A. Klug, K. E. O'Hara, S. M. DeSoto, C. P. Slichter, T. A. Friedmann, and D. M. Ginsberg,

ibid. **68**, 702 (1992); J. A. Martindale, S. E. Barrett, K. E. O'Hara, C. P. Slichter, W. C. Lee, and D. M. Ginsberg, Phys. Rev. B **47**, 9155 (1993).

[12] P. C. Hammel, M. Takigawa, R. H. Heffner, Z. Fisk, and K. C. Ott, Phys. Rev. Lett. **63**, 1992 (1989); M. Takigawa, J. L. Smith, W. L. Hults, Phys. Rev. B **44**, 7764 (1991); M. Takigawa and D. B. Mitzi, Phys. Rev. Lett. **73**, 1287 (1994).

[13] K. Ishida, Y. Kitaoka, N. Ogata, T. Kamino, K. Asayama, J. R. Cooper, and N. Athanassopoulou, J. Phys. Soc. Jpn. **62**, 2803 (1993).

[14] For a review of NMR data prior to 1990 see C. H. Pennington and C. P. Slichter, in *Physical Properties of High Temperature Superconductors II*, edited by D. M. Ginsberg (World Scientific, Singapore, 1990), pp. 269–367.

[15] F. Marsiglio, Phys. Rev. B **44**, 5573 (1991).

[16] R. Akis and J. P. Carbotte, Solid State Commun. **78**, 393 (1991).

[17] J. M. Chwalek, C. Uher, J. F. Whitaker, G. A. Mourou, J. Agostinelli, and M. Lelental, Appl. Phys. Lett. **57**, 1696 (1990).

[18] S. G. Han, Z. V. Vardeny, K. S. Wong, O. G. Symko, and G. Koren, Phys. Rev. Lett. **65**, 2708 (1990); S. G. Han, Z. V. Vardeny, O. G. Symko, and G. Koren, *ibid*. **67**, 1053 (1991).

[19] G. L. Eesley, J. Heremans, M. S. Meyer, G. L. Doll, and S. H. Liou, Phys. Rev. Lett. **65**, 3445 (1990).

[20] D. H. Reitze, A. M. Weiner, A. Inam, and S. Etemad, Phys. Rev. B **46**, 14309 (1992).

[21] W. Albrecht, Th. Kruse, K. Leo, and H. Kurz, Appl. Phys. A **56**, 463 (1993); W. Albrecht, Th. Kruse, and H. Kurz, Phys. Rev. Lett. **69**, 1451 (1992).

[22] D. Mandrus, L. Forro, D. Koller, C. Kendziora, and L. Mihály, Phys. Rev. B **46**, 8632 (1992).

[23] A. Sudbø, S. Chakravarty, S. Strong, and P. W. Anderson, Phys. Rev. B **49**, 12245 (1994).

[24] J. P. Lu, Mod. Phys. Lett. B **6**, 547 (1992).

[25] D. Thelen, D. Pines, and J. P. Lu, Phys. Rev. B **47**, 9151 (1993).

[26] Y. Itosh, H. Yasuoka, Y. Fujiwara, Y. Ueda, T. Machi, I. Tomeno, K. Tai, N. Koshizuka, and S. Tanaka, J. Phys. Soc. Jpn. **61**, 1287 (1992).

[27] P. M. Mankiewich, J. H. Scofield, W. J. Skocpol, R. E. Howard, A. H. Dayem, and E. Good, Appl. Phys. Lett. **51**, 1753 (1987); M. P. Siegal, J. M. Phillips, Y. F. Hsieh, and J. H. Marshall, Physica C **172**, 282 (1990); M. P. Siegal, J. M. Phillips, T. B. van Dover, T. H. Tiefel, and J. H. Marshall, J. Appl. Phys. **68**, 6353 (1990).

[28] M. P. Siegal, J. M. Phillips, R. B. van Dover, R. C. Farrow, T. H. Tiefel, and J. H. Marshall, J. Appl. Phys. **70**, 4982 (1991).

[29] D. J. Carlson, M. P. Siegal, J. M. Phillips, H. Tiefel, and J. H. Marshall, J. Mater. Res. **5**, 2797 (1990).

[30] M. van Exter and D. R. Grischkowsky, IEEE Trans. Microwave Theory Tech. **38**, 1684 (1990).

[31] D. H. Auston, in *Ultrafast Optical Pulses*, 4th ed., edited by W. Kaiser (Springer-Verlag, New York 1993), Chap. 5.

[32] D. C. Mattis and J. Bardeen, Phys. Rev. **111**, 412 (1958).

[33] W. Zimmerman, E. H. Brandt, M. Bauer, E. Seier, and L. Genzel, Physica C **183**, 99 (1991).

[34] J.-J. Chang and D. J. Scalapino, Phys. Rev. B **40**, 4299 (1989).

[35] A. J. Berlinsky, C. Kallin, G. Rose, and A.-C. Shi, Phys. Rev. B **48**, 4074 (1993).

[36] J. R. Schrieffer, *Theory of Superconductivity* (Addison-Wesley, New York, 1964).

[37] A. Frenkel, Phys. Rev. B **48**, 9717 (1993).

[38] A. Frenkel, M. A. Saifi, T. Venkatesan, P. England, X. D. Wu, and A. Inam, J. Appl. Phys. **67**, 3054 (1990).

[39] H. S. Carslaw and J. C. Jaeger, *Conduction of Heat in Solids* (Clarendon, Oxford, 1986), p. 75.

[40] D. T. Morelli, J. Mater. Res. **7**, 2492 (1992).

[41] M. Fardmanesh, M. Ihsan, K. Scoles, and A. Rothwarth, in *Superconductivity and Its Applications*, edited by H.-S. Kwok, D. T. Shaw, and M. J. Naughtan, AIP Conf. Proc. No. 273 (AIP, New York, 1993), p. 142.

[42] P. C. Michael, J. U. Trefny, and B. Yarar, J. Appl. Phys. **72**, 107 (1992).

[43] C. Uher, J. Supercond. **3**, 337 (1990); in *Physical Preoperties of High Temperature Superconductors III*, edited by D. M. Ginsberg (World Scientific, Singapore, 1991), pp. 159–283.

[44] S. Chakravarty, A. Sudbø, P. W. Anderson, and S. Strong, Science **261**, 337 (1993).

[45] P. W. Anderson, in *Superconductivity*, Proceedings of the ICTP Spring College in 1992, edited by P. Butcher and Y. Lu (World Scientific, Singapore, 1992).

[46] C. J. Gorter and H. G. B. Casimir, Phys. Z **35**, 963 (1934).